Chapter 3

AMS signal processing

The AMS signal is formed by electron impact ionization of gas from vaporization of single particles at a resistively heated surface near the quadrupole. In this section we develop a framework for converting this signal into aerosol size distributions, accounting for instrumental effects including lens transmission efficiency and single particle and/or chopper broadening. This section is especially important for studies of microphysical aerosol processes where the size distribution is changing, such as: nucleation of vapor to form new particles, condensation and evaporation of gas-phase species interacting with the particle surface, and coagulation (or coalescence) of particles to form larger particles.

In this treatment we assume that the sampled particles are pure and that only one m/z is being monitored. The approach can be easily generalized to multi-component aerosols since the instrument has demonstrated linear mass detection on particles of multiple species. A series of experiments performed on particle mixtures demonstrating this important result is presented in an appendix (A3.2) at the end of the chapter.

3.1 Absolute detection of particle size distributions

Because this section relies on the definition of many new symbols, we have put them all in the following table for easy access, including units and typical numerical values.

Quantity	Units	Symbol	Numerical
Electron charge	Coulombs	e	1.602×10^{-19}
Avogadro constant	molecules/mole	Av	6.022×10^{23}
Density of particle	ug/nm^3	ρ	$\sim 10^{-15}$
Specific gravity of particle	unitless	s	~ 1
Volume flowrate into AMS	(m^3 air)/s	Q	$\sim 10^{-4}$
Aerodynamic diameter	nm	D_a	10-1000
Geometric diameter	nm	D	10-1000
Molecular weight	g/mole	M	10-300
Transmission efficiency	unitless	ε_T	0-1
Ionization / extraction efficiency	unitless	ε_{ie}	$\sim 10^{-6}$
Electron multiplier gain	unitless	g	$\sim 10^6$
Current to voltage conversion	Ohms (volts/amp)	R	$\sim 10^6$
Voltage to signal conversion	bits/volt	Ω	$2^{12}/20$
Chopper period	seconds	T	$\sim 7 \times 10^{-3}$
Chopper duty cycle	unitless	∂	$\sim 2 \times 10^{-2}$
Duration of t_f step	seconds	Δ	$\sim 10^{-5}$
AMS signal	bits	S	-----
Ions per particle measurement	ions/particle	ipp	~ 100
Total particle mass loading	ug/m^3 air	M_{tot}	-----
Total particle number density	1/m^3 air	N_{tot}	-----
Threshold counts	1/m^3 air	N_c	-----
Signal to mass conversion	μg/m^3/bitsec	ϕ	~1e4

Quantity	Units	Symbol	Numerical
Particle flight length	m	l	0.382
Velocity calibration constant	nm	D^*	27.2
Velocity calibration constant	unitless	b	0.479
Gas velocity	m/s	Vg	592
Particle shape factor	unitless	β	~ 1
AMS histogram counts	1/cc	H	-----
Particle time of flight	seconds	t_f	~ 10^{-3}

3.1.1 TOF signal from a single ion

The conversion of AMS signal to mass and number distributions was originally summarized by Jayne et al., [2000]. In this section we present a more detailed derivation, leading to the same general result.

Particles incident on the heater are vaporized, and their constituent molecules are fragmented by electron impact ionization. These charged fragments are then filtered based on their mass to charge ratio. A single positive ion emerging from the quadrupole filter is then incident on the electron multiplier, resulting in a cascade of electrons emitted over a short time, τ. This constitutes an average current, I (Coulombs / s) persisting for the same duration:

$$< I >= \frac{ge}{\tau}$$

Here g is the multiplier gain and e is the charge of an electron. In the pre-amplifier this current is converted to an average voltage over the same duration:

$$< V >= R\frac{ge}{\tau}$$

Here, R is the resistance representative of the pre-amplifier. At the A/D board this voltage is converted to an average signal, S also persisting for the same time:

$$< S >= \Omega < V >= \frac{\Omega Rge}{\tau}$$

Here, Ω is the signal to voltage conversion factor. We can now rearrange and interpret the signal area of a single ion pulse measured in bit•seconds:

$$< S > \tau \equiv \int_0^{\tau} S(t_f)dt_f \cong \sum_{i=0}^{n} S_i\Delta = \Omega Rge \qquad (3.1)$$

Here n is the number of time steps in the pulse duration, τ, and Δ is the duration of a single time step. Equivalently, as is delivered by the "info" wave in the AMS software, we may write the number of bit•steps per single ion as $\frac{\Omega Rge}{\Delta}$. Since the AMS software performs this calculation to deliver the *ipp* (ions per particle) measurement, a proper measurement of 1 ion/ion insures (by definition) that the gain is correct at that particular value of the multiplier voltage.

3.1.2 Aerosol mass concentration (loading) from the time of flight (TOF) signal

We are now in position to convert the number of bits at a given t_f to the appropriate dm/dt_f value needed for absolute mass detection. Our strategy will be to work backwards from the observed signal area to the mass concentration (loading).

Numerically, the signal is an array, with an associated TOF array of the same dimension. For the ith point we have, $t_{f_i} = \Delta i$. The integral of the total signal over the

full range of t_f values can be converted to the number of ions incident on the multiplier in a given chopper period:

$$\frac{1}{\Omega Rge}\sum_{i=0}^{N} S_i \Delta$$

These ions represent the number of molecules resulting from particle vaporization events over one chopper period,

$$\frac{1}{\varepsilon_{ie}\Omega Rge}\sum_{i=0}^{N} S_i \Delta$$

We can write this in terms of total μg vaporized in T as:

$$\frac{M}{A_v \varepsilon_{ie}\Omega Rge}\sum_{i=0}^{N} S_i \Delta \qquad (3.2)$$

The mass current incident on the chopper wheel is $M_{tot}Q$. Of this, only δTQM_{tot} μg passes through the chopper slit in one cycle. Through mass balance we equate this quantity to the quantity given by eq. 3.2 above, such that:

$$M_{tot} = \phi\sum_{i=0}^{N} S_i \Delta \quad where \quad \phi \equiv \frac{M}{Q\partial TA_v \varepsilon_{ie}\Omega Rge} \qquad \text{ug m}^{-3}\ \text{s}^{-1}\ \text{bit}^{-1} \qquad (3.3)$$

Eq. 3.3 links the total mass concentration (loading) of particles sampled into the AMS inlet to the integrated signal in TOF space. From here we may generalize to construct the mass distribution, dm/dt_f, by re-writing the previous expression for total mass loading as:

$$M_{tot} = \int_0^{\infty} \frac{dm}{dt_f} dt_f = \sum_{i=0}^{N} \frac{m_i}{\Delta}\Delta = \phi\sum_{i=0}^{N} S_i \Delta$$

By inspection, we have for the ith t_f bin:

$$\frac{dm}{dt_f} = \frac{m_i}{\Delta} = \phi S_i \qquad (3.4)$$

This expression links the observed signal in the i^{th} t_f bin to the dm/dt_f of the aerosol ensemble at that corresponding t_f. We note that this mass distribution represents ensembles in the instrument *after* passing through the lens and the chopper. In many applications, this is a sufficient approximation for the true mass distribution present at the AMS sampling inlet. An approach for obtaining more accurate representations of the mass distribution is treated in a later section.

3.1.3 The mass calibration factor for the TOF signal

Calculating accurate mass or size distributions from the AMS signal requires that we know ϕ to high accuracy. Only two parameters, ε_{ie} and g, in the expression for ϕ must be experimentally determined. The gain, g can be found with a series of single ion measurements. To determine the detection efficiency, ε_{ie} in the absence of a CPC/DMA setup, one must sample a significant number of single particles while fulfilling two requirements: 1) the particles must be large enough to cross the threshold most of the time (typically 100 ions), and 2) the average time between particle arrivals at the heater must be greater than the vaporization time. We can approximate the upper limit number density at which coincidence is likely by requiring the inverse arrival frequency of the particles to be longer than the particle vaporization time yielding, $N_{max} \sim (Q\tau_{vap})^{-1}$. Condition 2 is necessary to avoid particle coincidence, which would lead to an overestimate of the number of ions per particle. Also, one cannot insure condition 2 without first satisfying condition 1. Bubbling with a frit through a solution of the species of interest can produce polydisperse (containing a wide range of particle sizes) distributions of most liquid particles, and number densities can be controlled with dilution. The task then is to record ions/particle for a few different particle sizes

(typically greater than 300 nm), with a range that is as small as possible (i.e. +/- 5 nm) while still allowing acceptable statistics. The ionization / extraction efficiency, representing the number of ions extracted per molecule vaporized will then be given by:

$$\varepsilon_{ie} = \frac{6(ipp)M}{\rho \pi D^3 A_v} \tag{3.5}$$

3.2 Display options for aerosol size distributions

In the following sections extensive use is made of transformations enabling passage from one distribution space to another. This is not only important from the standpoint of signal processing, but also as a general tool to link experimental and modeling outputs. In addition, displaying aerosol distribution dynamics in different ways sometimes reveals important aspects of the underlying physics. Changes that appear insignificant in number space for example may be quite dramatic in volume (or mass) space. Transformations can be used to change both the independent and dependent variable. We may, for example wish to convert a distribution of number over sizes (*dN/dD*) to a distribution of number over mass (*dN/dm*), requiring a change in the independent variable. At other times we may be interested in changing a distribution of number over sizes (*dN/dD*) to a distribution of mass over sizes (*dM/dD*) requiring a change in the dependent variable. Specific methods for transforming particle size distributions are also available in Seinfeld and Pandis [1998]. In this section, we present a more general method for transforming distributions from one form to another while maintaining their initial properties.

We define a general distribution $f_y(x)$ as the following:

$$f_y(x) \equiv \frac{dY}{dx} \tag{3.6}$$

All such distributions have the property that $f_y(x)dx$ represents the amount[a] of Y (i.e. number, surface area, or mass) located within a given infinitesimal range of x (i.e. number, surface area, or mass), from x to $x + dx$. It follows that integration of such distributions over all space will yield the total amount of Y contained within the ensemble, which we denote Y_0:

$$\int_{x=0}^{\infty} f_y(x)dx = Y_0 \tag{3.7}$$

This might, for example, represent the total number of particles, summed over all possible diameters. Should we desire changing the independent variable, from say x_1 to x_2, the total amount of Y integrated over either space must still equate to Y_0. The equality must also hold over each infinitesimal range:

$$f_1(x_1)dx_1 = f_2(x_2)dx_2 \tag{3.8}$$

We may therefore write the transformed function as:

$$f_2(x_2) = f_1(x_1)\frac{dx_1}{dx_2} \tag{3.9}$$

It is apparent that we are simply re-affirming the chain rule[1] in conserving Y upon transforming f_1 when we write:

$$f_2(x_2) \equiv \frac{dY}{dx_2} = \frac{dY}{dx_1}\frac{dx_1}{dx_2} \tag{3.10}$$

We may generalize a transformation involving both the independent and dependent variable using the chain rule in a similar fashion, as in:

$$f_{y_2}(x_2) = \frac{dY_2}{dx_2} = \frac{dY_1}{dx_1}\frac{dx_1}{dx_2}\frac{dY_2}{dY_1} = f_{y_1}(x_1)\frac{dx_1}{dx_2}\frac{dY_2}{dY_1} \tag{3.11}$$

[a] Were we to normalize such a function, f would represent the fraction of quantity Y contained in the same range.

Eq. 3.11 simultaneously transforms Y_1 to Y_2 and x_1 to x_2 while maintaining the property given by eq. 3.8.

Due to the popularity of the lognormal distribution (see below), it is common to display aerosol distributions over x in log-space. Such plots show symmetric modes whenever a log-normal distribution is present. Since $d\ln x/dx = 1/x$ and $d\log x/dx = 1/2.303x$, any distribution in x-space can be converted to a distribution in $\ln x$ or $\log x$-space through the following:

$$\frac{dY}{d\ln x} = \frac{dx}{d\ln x}\frac{dY}{dx} = x\frac{dY}{dx} \tag{3.12}$$

$$\frac{dY}{d\log x} = \frac{dx}{d\log x}\frac{dY}{dx} = 2.303x\frac{dY}{dx} \tag{3.13}$$

In numerical modeling the choice of distribution on which to carry out calculations is sometimes critical. Numerical coagulation studies, for example, proceed from eq. 6.20 (see ch. 6) where dN/dm is the chosen distribution ($dN/d\ln m$ is also common). Here, we develop transformations using the method outlined above to pass from both of theses quantities to $dN/d\log D$. Other transformations can be obtained in a similar fashion. For the case of $dN/d\ln m$ we begin with the following:

$$\frac{dN}{d\log D} = \frac{d\ln m}{d\log D}\frac{dN}{d\ln m}$$

Using eq. 3.12 and 3.13, we have:

$$\frac{d\ln m}{dm} = \frac{1}{m} \quad \text{and} \quad \frac{d\log D}{dD} = \frac{2.303}{D}$$

and thus:

$$\frac{d\ln m}{dm}\frac{dD}{d\log D} = \frac{1}{m}\frac{D}{2.303}$$

or

$$\frac{d\ln m}{d\log D} = \frac{1}{m}\frac{D}{2.303}\frac{dm}{dD} \qquad \text{with} \qquad \frac{dm}{dD} = \frac{\rho\pi D^2}{2} \tag{3.14}$$

such that upon gathering terms:

$$\frac{dN}{d\log D} = \frac{3}{2.303}\frac{dN}{d\ln m} \tag{3.15}$$

Another useful conversion is from *dN/dm* to *dN/dlogD*. Once again using eq. 3.13:

$$\frac{dN}{d\log D} = 2.303D\frac{dN}{dD} = 2.303D\frac{dm}{dD}\frac{dN}{dm}$$

Combining this with eq. 3.14 above, we have:

$$\frac{dN}{d\log D} = \frac{2.303\rho\pi D^3}{2}\frac{dN}{dm} \tag{3.16}$$

3.3 Estimation of various distributions from TOF signal

In this section we describe a procedure for obtaining estimates of various distributions from the AMS signal, ignoring the effects of single particle and chopper broadening. A more accurate treatment for the signal processing is outlined in the next section.

Due to non-unity lens transmission, we must modify eq. 3.4 to get a closer representation of the mass distribution being sampled into the AMS inlet. The signal at a given t_f is proportional to the mass distribution of an aerosol ensemble at that point in t_f space divided by the lens transmission efficiency (see sec. 2.2):

$$\frac{dM}{dt_f} = \frac{\phi S(t_f)}{\varepsilon_T(t_f)} \tag{3.17}$$

Conversion to a mass distribution in geometric diameter space is given by the transformation (see eq. 3.11):

$$\frac{dM}{dD} = \frac{dM}{dt_f}\frac{dt_f}{dD_a}\frac{dD_a}{dD} \tag{3.18}$$

The aerodynamic diameter is given by:

$$D_a = s\beta D \qquad \text{and} \qquad \frac{dD_a}{dD} = s\beta \tag{3.19}$$

The aerodynamic diameter is defined as the diameter of a unit density sphere having the same settling velocity (the terminal velocity in free fall) as the particle. Particles more dense than water will have aerodynamic diameters larger than their geometric diameters. Also in eq. 3.19, β represents the shape factor of the particle, with a value of unity for spherical particles. Unless a particle has a needle-like geometry, non-spherical particles will typically have $\beta < 1$. Taking the expression for particle velocity as a function of aerodynamic diameter[2], t_f can be written as a function of aerodynamic diameter:

$$t_f = \frac{l(1+(D_a/D^*)^b)}{V_g} \tag{3.20}$$

such that

$$\frac{dt_f}{dD_a} = \frac{lb}{V_g (D^*)^b} D_a^{\,b-1} \tag{3.21}$$

So the expression for the mass distribution becomes:

$$\frac{dM}{dD} = \frac{\phi s\beta\kappa D_a^{\,b-1} S(t_f)}{\varepsilon_T(t_f)} \qquad \kappa \equiv \frac{lb}{V_g (D^*)^b} \tag{3.22}$$

From here other distributions can be obtained:

$$\frac{dN}{dD} = \frac{1}{m_p}\frac{dM}{dD} = \frac{6}{\rho\pi D^3}\frac{dM}{dD} \tag{3.23}$$

$$\frac{dS}{dD} = \pi D^2 \frac{dN}{dD} \tag{3.24}$$

In eq. 3.24, S represents the total surface area of the aerosol ensemble per unit volume of air.

Histogram counts as a verification of mass calibration

Processing of the histogram is independent of mass calibration and should match the above distributions in the limit of large sizes where the likelihood of crossing a threshold is high. Conversion of the histogram, H which is counts/cc in a given t_f bin to a number distribution is straightforward (from eq. 3.11):

$$\frac{dN_c}{dD} = \frac{dN_c}{dt_f}\frac{dt_f}{dD_a}\frac{dD_a}{dD} \tag{3.25}$$

The only new term in this expression is readily approximated since the time steps are much smaller than the chopper period:

$$\frac{dN_c}{dt_f} \cong \frac{H(t_f)}{\Delta} \tag{3.26}$$

such that

$$\frac{dN_c}{dD} = \frac{s\beta\kappa\, H(t_f) D_a^{\,b-1}}{\Delta} \tag{3.27}$$

Comparison of eq. 3.27 and eq. 3.23 (using 3.22) constitutes a check of the mass calibration, since in the limit of large sizes with negligible coincidence they should be identical.

3.4 Chopper and single particle broadening

As the aerosols impinge upon the chopper, they are sampled through a slit of finite width, open for a known duration. The aerosols passing through the chopper over this duration have a range of starting times with respect to their t_f. The result of this effect is to spread the signal in t_f space leading to a broadened mass distribution compared to the distribution actually sampled into the instrument. We can think of this process as an integrated system response to a series of impulses. Mathematically, we can reconstruct the overall system response (output) through superposition of the individual responses to each impulse (input) using the *convolution*[3]. In this way, we write the output mass distribution, $dm/dt_f = m_{AMS}(t_f)$ as a function of the input mass distribution, assuming a certain chopper response function, $c(t_f)$.

$$m_{AMS}(t_f) = \int_{\tau=0}^{\tau=t_f} m(\tau)c(t_f - \tau)d\tau \tag{3.28}$$

The response function (i.e. for chopper broadening) links the system response to an impulse. A response function for chopper broadening may be derived from first principles, but depends on the detailed interaction between the particle beam and the chopper. In this treatment we only suggest an approximate function, of which a parameterized version is appropriate for many applications. If, for example, an infinitesimally small segment of $dM/dt_f = m(t)$ centered on t constitutes the impulse, we may estimate the response to be $m'(t)$ given by:

$$m'(t) = \frac{\Delta}{\Lambda} m(t) \tag{3.29}$$

Here Λ is the opening time of the chopper slit and Δ is the t_f step size. So the impulse effect of chopper broadening is to take an amount of mass, $m(t)$ at a given t_f, t and spread

it out across t_f space from t - $\Lambda/2$ to $t + \Lambda/2$. The magnitude decreases to *m'(t)* in order to conserve mass. In practice, we are not constrained to assume that the magnitude of the transfer function be any set value, as long as mass is conserved in the overall distribution before and after convolution. Defining the magnitude of the chopper response function to be θ, we may now define the chopper broadening function to be used in eq. 3.28 as:

$$\begin{aligned} c(t) &= \theta \quad t - \Lambda/2 < t_f < t + \Lambda/2 \\ c(t) &= 0 \quad t_f = anywhere\ else \end{aligned} \tag{3.30}$$

3.4.1 Outline of a rigorous approach

For data analysis we must compare expected mass or number distributions with the data. Ideally we would solve eq. 3.28 for $m(t_f)$ for comparison with theory. One strategy for obtaining $m(t_f)$ involves the use of Fourier and inverse Fourier transforms. We outline that strategy here briefly. Taking the Fourier transform of both sides of eq. 3.28 we have:

$$F[m_{AMS}(t_f)] = F[\int_{\tau=0}^{\tau=t_f} m(\tau)c(t_f - \tau)d\tau] = F[m \otimes c] \tag{3.31}$$

The special notation on the right-hand side is simply used as shorthand for the convolution. An important property of the convolution is that its Fourier transform is equal to the product of the Fourier transforms of each convolved function, such that:

$$F[m_{AMS}(t_f)] = F[m \otimes c] = F[m(t_f)]F[c(t_f)] \tag{3.32}$$

or

$$M_{AMS}(\omega) = M(\omega)C(\omega) \tag{3.33}$$

Eq. 3.33 reflects the fact that functions of time convert to different functions of frequency once they are transformed. We may now rearrange and take the inverse Fourier transform:

$$m(t_f) = F^{-1}[\frac{M_{AMS}(\omega)}{C(\omega)}] \tag{3.34}$$

It is therefore, in principle, mathematically possible to deconvolve the AMS output and recover distributions as sampled into the inlet. In practice, since $c(t_f)$ is difficult to derive, it is best obtained empirically. To do so, one must supply a known function for $m(t_f)$ (i.e. by using a DMA/CPC arrangement). The observed $m_{AMS}(t_f)$ can then be used as in the procedure above to determine $c(t_f)$. Since the chopper broadening function is independent of the particular distribution, it can be used for all subsequent determinations of $m(t_f)$ for different systems. Also, this procedure would need to be repeated for the single particle response function[b].

Another attractive feature of this approach is its comparatively low computational cost. Once in possession of $c(t_f)$ (empirical or derived), the two transforms required to extract $m(t_f)$ cost on the order of $NlnN$ calculations, where N is the number of time steps in $m_{AMS}(t_f)$. By contrast, one convolution costs on the order of N^2, and in the case where a curve fitting routine such as that described below is used, on the order of 10^2 convolutions will be calculated per fit. The computational cost of brute force convolution curve fitting is therefore $10^2N^2/NlnN$ times that of the Fourier transform approach. For dm/dt_f arrays with 10^3 points, this represents a factor of ~10^4. For large data sets such as those encountered in field work, use of the Fourier transform method may constitute significant computational savings[c].

[b] Convolution is associative, which means that we may convolve the chopper function first and then convolve the output with the single particle function or vice versa and still achieve the same result.

[c] This may be circumvented with faster processing speed.

Practical application of the method may however prove difficult, especially in the case of data with significant noise, since information having frequencies higher than the response function will be lost. Some recent work done on inversion of DMA data by R. Flagan and co-workers may prove applicable in this regard[d].

3.4.2 The curve-fitting method

If assumptions can be made about the distributions, we may proceed in a more straightforward fashion than that outlined in the rigorous approach. Our fitting procedure begins with assuming that the distributions can be represented with a sum of *n* lognormal particle size distributions (see below), with *3n* total fitting parameters. We begin by converting the initial guessed mass or number distribution to dM/dt_f space. We then account for lens transmission losses as the particles are aerodynamically focused into the instrument. The newly obtained dM/dt_f is then convolved with the chopper and single particle broadening functions. The final output is then compared to actual data, and the process is repeated iteratively to achieve the fit. An example is shown in fig. 3-1, below.

Conversion of number distributions to mass distributions in TOF space

For processes whose dynamics are driven by number distributions (such as coagulation), we must fit theoretical *dN/dlogD* to measured dM/dt_f. The transformation proceeds from (see eq. 3.11):

$$\frac{dM}{dt_f} = \frac{dM}{dD}\frac{dD}{dD_a}\frac{dD_a}{dt_f} \tag{3.35}$$

Proceeding as before we can show:

$$\frac{dM}{dt_f} = \frac{v_g}{lb}\left(\frac{D^*}{s\beta}\right)^b D^{1-b}\frac{dM}{dD} \qquad (\text{ug m}^{-3}\ \text{s}^{-1}) \tag{3.36}$$

[d] Personal communication.

We also have:

$$\frac{dM}{dD} = m_p \frac{dN}{dD} = \frac{\rho\pi D^3}{6}\frac{dN}{dD} = \frac{\rho\pi D^3}{6}\frac{1}{2.303D}\frac{dN}{d\log D}$$

such that upon gathering terms we write:

$$\frac{dM}{dt_f} = \frac{\pi}{(6)(2.303)}\eta D^{3-b}\frac{dN}{d\log D} \tag{3.37}$$

where

$$\eta \equiv \frac{\rho v_g}{lb}\left(\frac{D^*}{s\beta}\right)^b \tag{3.38}$$

We note that the particle shape factor and specific gravity must be known before this transformation can be performed.

Eq. 3.37 represents the size distribution before sampling into the lens. Using the lens transmission function, written as a function of t_f (as described in sec. 2.2.1), we can write the distribution actually incident on the chopper as:

$$\frac{dM}{dt_f} = \varepsilon_T(t_f)\frac{\pi}{(6)(2.303)}\eta D^{3-b}\frac{dN}{d\log D} \tag{3.39}$$

This preliminary dM/dt_f is then convolved with chopper and single particle functions and compared to the raw dM/dt_f taken from the AMS signal (given by eq. 3.4, above). Adjustments are then made to the parameters describing *dN/dlogD* and the process is continued until a fit is achieved (see fig. 3-1).

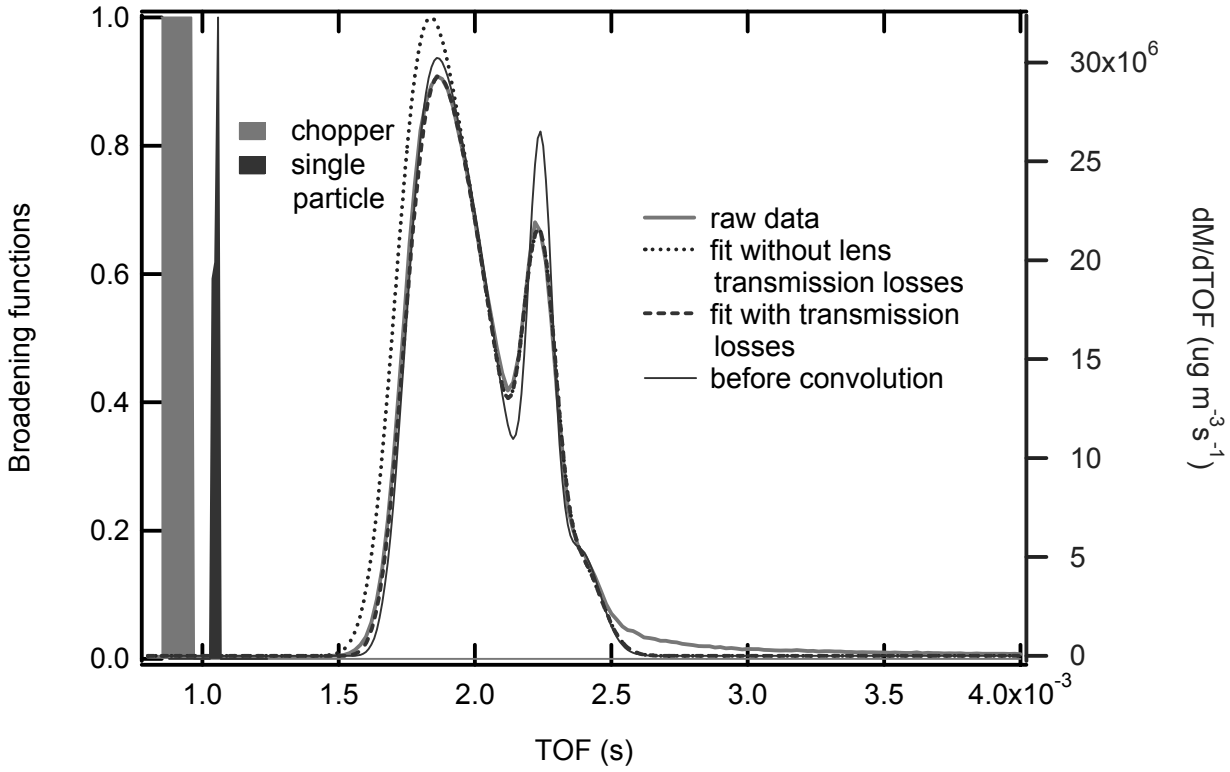

Figure 3-1: Sample fit using the curve-fitting method applied to a distribution of coagulating sulfuric acid particles.

The fit in fig. 3-1 shows the effect of non-unity transmission as well as that of chopper broadening. The dotted line indicates that there were more particles at smaller sizes than were actually observed. The sharpness of the second peak in the distribution before convolution reveals the effect of chopper broadening when it is compared to the raw data (thick gray line).

Chapter 3 Appendix

A3.1 Aerosol size distribution functions

In this section we briefly discuss the properties of two distributions with expected applicability to aerosol ensembles. The curve fitting method described above relies on an assumption of the functional form of a distribution, and it is common in field studies as well, to simplify aerosol size data potentially involving many species, by exploiting the compactness of such distribution functions.

The log-normal distribution

A particularly popular functional form for distributions in aerosol studies is the log-normal[4] distribution. Substituting the independent variable in a normal (Gaussian) distribution with its log yields the log-normal distribution:

$$\frac{dN}{d\log D} = \sum_{i=1}^{n} \frac{N_i}{\sqrt{2\pi}\log\sigma_i} \exp\left(-\frac{(\log D - \log \overline{D}_i)^2}{2\log^2 \sigma_i}\right) \tag{3.40}$$

For any given mode, *i*, there are three parameters describing the distribution within that mode: N_i is the total number of particles within mode *i*, $\overline{D}_i$, is the median diameter, and σ_i is the geometric standard deviation. It can be shown that 67% of all the particles in the i^{th} mode have diameters between $\overline{D}_i / \sigma_i$ and $\overline{D}_i \sigma_i$, and 95% of all the particles lie in the range between $\overline{D}_i / 2\sigma_i$ and $2\overline{D}_i \sigma_i$[5]. Here *n* is the number of log-normal distributions to be superimposed. Given a function representing the number distribution, the distributions in surface area and mass space are given by:

$$\frac{dS}{d\log D} = \pi D^2 \frac{dN}{d\log D} \tag{3.41}$$

$$\frac{dM}{d\log D} = \rho\frac{\pi D^3}{6}\frac{dN}{d\log D} \tag{3.42}$$

An advantage of the lognormal assumption is that it is straightforward to pass from number density to both mass and surface area densities, without performing the laborious point-by-point transform outlined above. It can be shown[6] (Seinfeld, pg. 425) that if a size distribution is log-normally distributed in number, it will also be log-normally distributed in both surface area and mass, with the same geometric standard deviation, σ. Furthermore, the median diameter in each space can be found from the median diameter in number space and σ (Seinfeld, p. 425):

$$\ln \overline{D}_x = \ln \overline{D} + k \ln^2 \sigma \tag{3.43}$$

This equation in *ln* space is applicable even for standard deviations, σ obtained from fits in *log* space, since *dN/dlogD* and *dN/dlnD* differ only by a multiplicative constant. Here, $\overline{D}$ is the median diameter in number density space, $\overline{D}_x$ is the median diameter in either surface area or mass density space, and *k* is 2 or 3 for surface or mass diameters respectively. We may therefore write each distribution functionally based solely on the parameters from the number density distribution:

$$\frac{dX}{d\log D} = \sum_{i=1}^{n} \frac{X_i}{\sqrt{2\pi}\log\sigma_i} \exp\left(-\frac{(\log D - \log \overline{D}_{x,i})^2}{2\log^2 \sigma_i}\right) \tag{3.44}$$

Here *X* is either mass, *M* or surface area, *S*, with $\overline{D}_x$ given by eq. 3.38. To find *M* or *S* for a given mode, one needs the average diameter of that mode. For a lognormal distribution, it can be shown that the average diameter in the ith mode is given by:

$$< D_{x,i} >= \overline{D}_{x,i} \exp\left(\frac{\ln^2 \sigma_i}{2}\right) \tag{3.45}$$

The extreme-value function

A distribution less cited in the aerosol literature but well known from probability theory is the extreme value function (also known as the Fisher Tippett function of type I)[7]. We have found this distribution to be especially useful in fitting soot mass distributions from a propane-generated source. A mass distribution having an extreme-value representation is given by:

$$\frac{dM}{dD} = \frac{M}{\beta}\exp(y - e^{y}) \tag{3.46}$$

with

$$y \equiv \frac{\alpha - D}{\beta}$$

Here, M is the total mass density of the particle ensemble. The mean mass-weighted diameter is given by $\alpha + \gamma\beta$, where γ is Euler's constant ($\gamma = 0.5772\ldots$). The variance is given by: $\langle D^2 \rangle = (\pi\beta)^2/6$. We note that this function needs as many variables to describe a distribution as a log-normal, and would only be chosen as a substitute function if it enabled a better fit than the lognormal.

A3.2 Mass detection of multi-component particles

Signal to mass calibration of particles of one component (see above) enables absolute detection of size and mass distributions of that species for laboratory and field studies. However, particles encountered in the atmosphere rarely consist of only one component. Likewise during chemical kinetics experiments (see ch. 5) on aerosols, the particle composition is changing, often involving product species for which the identity is unknown. Because the intermolecular forces that hold the particle together (before it is

vaporized by the heater) change with composition, the mass calibration (or detection efficiency) of a given species may vary with particle composition. This is especially important for particles composed of species with very different thermal properties. We have designed a series of experiments aimed at detecting such *matrix effects* on the AMS mass detection. The absence of matrix effects must be demonstrated in order to use calibration factors from pure species on those same species present in multi-component particles.

Experiments were performed on particle mixtures consisting of up to four components. Particle ensembles were generated from the atomizer and then size-selected using a Differential Mobility Analyzer (DMA). Mixing known masses of various species in the atomizer solution created particle mixtures of varying composition. Since the atomizer solution was well mixed and atomized droplets have large volumes ($\sim 10^{-1}$ μm^3) relative to density fluctuation length-scales in solution, the particles reflect the same mole fractions as were present in solution. Examples of some of the mixtures for which particles were sampled include: NH_4Br and NH_4Cl, $(NH_4)_2SO_4$ and NH_4NO_3, and an organic/inorganic mixture of oxalic acid and NH_4Br. Experiments were also done on particles consisting of four different species of salts. The error bars in these plots reflect the standard deviation in the ions per particle measurement (see ch. 5). For our present purposes, the ions per particle measurement is an indicator of the relative mass of a given species that is detected in particles of a given size.

The results of these experiments are summarized in the plots in figs. A3-1 through A3-4.

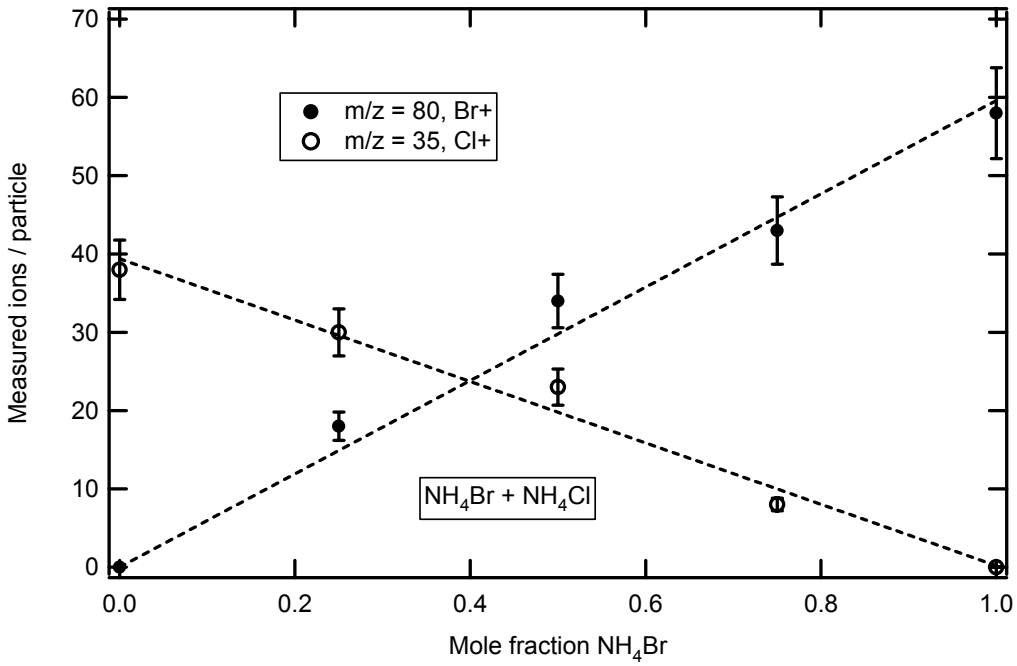

Figure A3-1: Demonstrated linear detection efficiency for a salt mixture of NH_4Br and NH_4Cl.

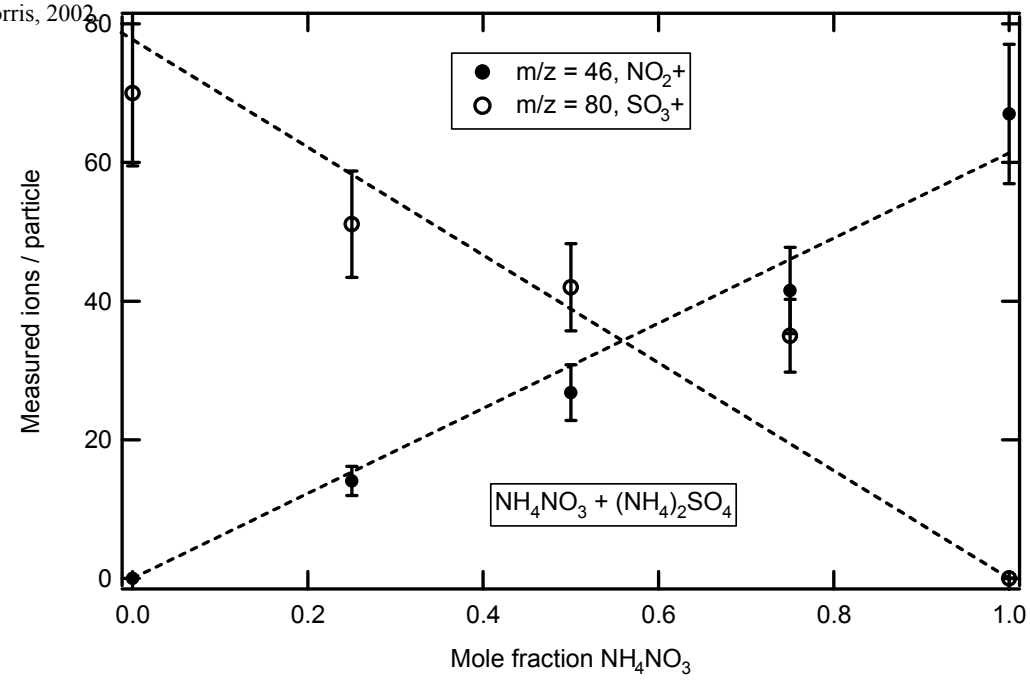

Figure A3-2: Demonstrated linear detection efficiency for a salt mixture of $(NH_4)_2SO_4$ and NH_4NO_3.

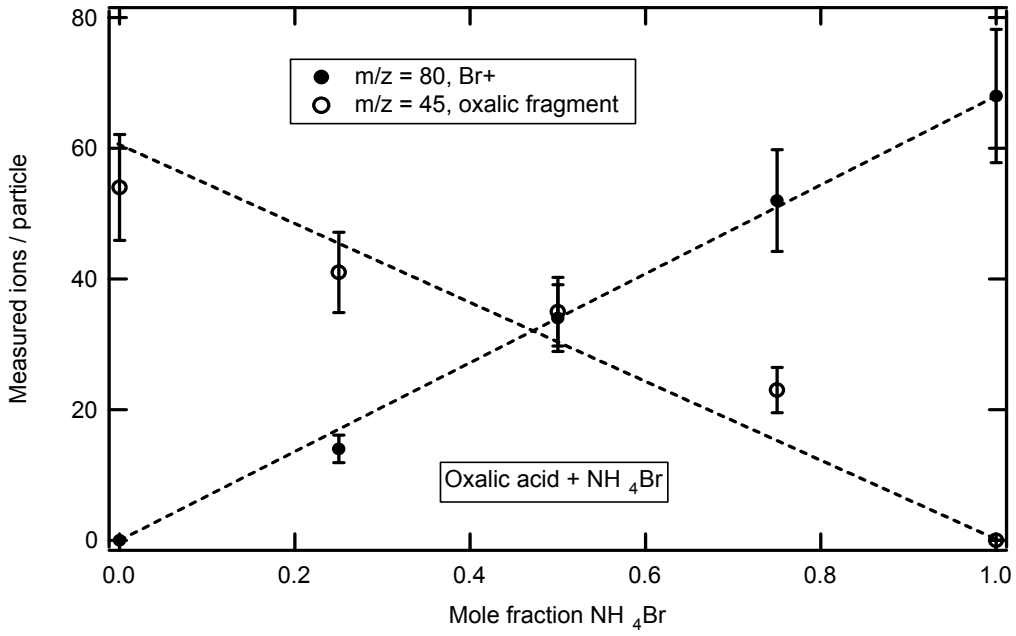

Figure A3-3: Demonstrated linear detection efficiency for an organic / salt mixture of oxalic acid and NH_4Br.

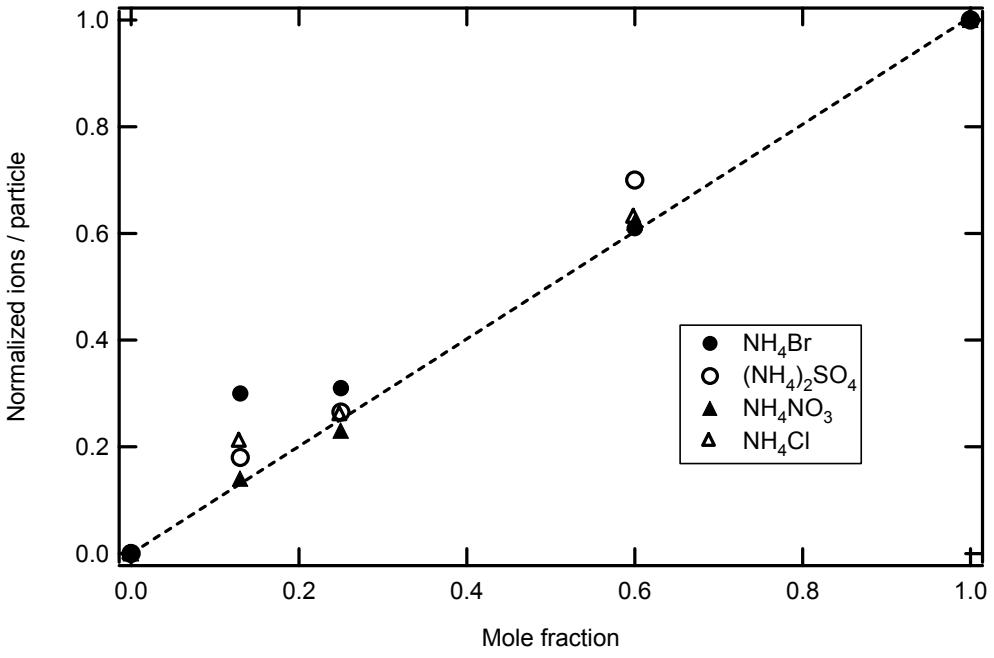

Figure A3-4: Demonstrated linear detection efficiency for a mixture of four different salts. Here, the error bars are not shown to facilitate viewing.

As is evident in these plots, linear mass detection is demonstrated within experimental error on several binary mixtures. There is some significant error however in the case of 4-component mixtures, as seen in fig. A3-4, in the case of ammonium bromide. We encourage further experimentation on complicated mixtures, especially those mixtures representative of compositions likely to be found in the atmosphere. Demonstrated linear detection efficiency on such particles should precede more ambitious experiments aimed at probing the kinetics and microphysics of particles with multiple components.

Chapter 3 References

[1] G. F. Simmons, *Calculus with Analytic Geometry*, (McGraw Hill, 1996).

[2] J. Jayne, D. Leard, Z. Zhang, P. Davidovits, C. Kolb, and D. Worsnop. *Aerosol Sci. Technol*., **33**, 49 (2000).

[3] R. H. Cannon, *Dynamics of Physical Systems*, (McGraw Hill, New York, 1967).

[4] J. H. Seinfeld and S. N. Pandis, *Atmospheric Chemistry and Physics*, (Wiley, New York, 1998).

[5] Seinfeld and Pandis, p. 423.

[6] Seinfeld and Pandis, p. 425.

[7] *Hanbook of Mathematical Functions*, (Dover, 1968).